Available online at www.sciencedirect.com

SciVerse ScienceDirect

journal homepage: www.elsevier.com/locate/he

Comparative study of CuO supported on CeO_2, $Ce_{0.8}Zr_{0.2}O_2$ and $Ce_{0.8}Al_{0.2}O_2$ based catalysts in the CO-PROX reaction

A. Arango-Díaz [a], J.A. Cecilia [a], E. Moretti [b], A. Talon [b], P. Núñez [c], J. Marrero-Jerez [c], J. Jiménez-Jiménez [a], A. Jiménez-López [a], E. Rodríguez-Castellón [a,*]

[a] Departamento de Química Inorgánica, Facultad de Ciencias, Universidad de Málaga, 29071 Málaga, Spain
[b] Dipartimento di Scienze Molecolari e Nanosistemi, Università Ca' Foscari Venezia, Via Torino 155/b, 30172 Mestre-Venezia, Italy
[c] Departamento de Química Inorgánica, Universidad de La Laguna, La Laguna, Spain

ARTICLE INFO

Article history:
Received 9 January 2013
Received in revised form
9 April 2013
Accepted 12 April 2013
Available online 11 May 2013

Keywords:
Nanocrystalline CeO_2
Freeze-drying method
Copper oxide
Preferential CO oxidation
Hydrogen

ABSTRACT

CuO supported on CeO_2, $Ce_{0.8}Zr_{0.2}O_2$ and $Ce_{0.8}Al_{0.2}O_2$ based catalysts (6%wt Cu) were synthesized and tested in the preferential oxidation of CO in a H_2-rich stream (CO-PROX). Nanocrystalline supports, CeO_2 and solid solutions of modified CeO_2 with zirconium and aluminum were prepared by a freeze-drying method. CuO was supported by incipient wetness impregnation and calcination at 400 °C. All catalysts exhibit high activity in the CO-PROX reaction and selectivity to CO_2 at low reaction temperature, being the catalyst supported on CeO_2 the more active and stable. The influence of the presence of CO_2 and H_2O was also studied.

1. Introduction

Fuel cells have emerged as one of the most important power generation systems. Proton Exchange Membrane Fuel Cells (PEMFCs) have been intensively studied due to the increasing interest on the development of efficiency, and environmentally friendly ways of energy generation [1].

Nanomaterials are systems that contain particles with 1-D in the nanometer range. Nowadays, there is a growing interest due to the unusual properties that are exhibited by these materials. One of the most relevant is the surface effect that dominates the thermodynamics and energetic of the particles. This factor leads to nanocrystals adopting different morphologies and to the variation in the catalytic activity [2].

Hydrogen-rich gas streams production mainly uses steam reforming of hydrocarbons followed by the water–gas shift reaction [1,3]. The resulting gas mixtures contain about 1% CO, but the CO concentration must be reduced below 10 ppm because the Pt anode of PEMFCs is highly sensitive to CO poisoning [3]. One of the most straightforward and cost effective methods to decrease the CO concentration down is the preferential catalytic oxidation of CO (CO-PROX) [4]. The

* Corresponding author. Tel.: +34 952131873; fax: +34 952131870.
E-mail addresses: castellon@uma.es, estrella.aguado@gmail.com (E. Rodríguez-Castellón).
0360-3199/$ – see front matter
http://dx.doi.org/10.1016/j.ijhydene.2013.04.062

catalysts for CO-PROX must be highly selective and stable in a wide temperature range, tolerant to CO_2 and H_2O. One of the most investigated catalytic systems for CO-PROX is CuO supported on CeO_2. CuO/CeO_2 based oxide systems appear to be selective, thermally stable and low cost [5–8]. The redox behavior of $CuO–CeO_2$ can be increased by the addition of heteroatoms (i.e., Zr, Al) enhancing the synergistic redox properties and its oxygen-storage capacity [8–11].

In this paper, the preparation of nanocrystalline ceria-based materials by freeze-drying method which presents advantages as the absence of diffusion process in their synthesis, their use as supports of copper oxide and their performance in the CO-PROX reaction at low temperatures (65–190 °C) are described.

2. Experimental

2.1. Sample preparation

2.1.1. CeO_2 and modified CeO_2 preparation

Polycrystalline CeO_2, $Ce_{0.8}Zr_{0.2}O_2$ and $Ce_{0.8}Al_{0.2}O_2$ were synthesized by freeze-drying method, using $Ce(NO_3)_3{\cdot}6H_2O$, $ZrO(NO_3)_2{\cdot}6H_2O$ and $Al(NO_3)_3{\cdot}12H_2O$ as precursors. The reagents were dissolved in water and then ethylenediaminetetraacetic acid (EDTA) was added as complexing agent to prevent precipitation in a 1:1 ligand:metal molar ratio. The pH of the solution was adjusted at 7–8 by adding aqueous ammonia. The solution was flash frozen dropwise into liquid nitrogen and dried in a freeze-dryer for 3 days. The amorphous precursor was calcined at 300 °C for 2 h to prevent rehydration and to eliminate the organic matter. Finally, the powders were calcined at 600 °C for 5 h. Under these synthesis conditions, crystallization of CeO_2 and solid solutions $Ce_{0.8}Zr_{0.2}O_2$ and $Ce_{0.8}Al_{0.2}O_2$ powders to a single phase were achieved [12].

2.1.2. $CuO–CeO_2$ and $CuO–CeO_2$ based catalysts preparation

Copper containing catalysts were prepared by incipient wetness impregnation of the supports with a solution of copper(II) acetate (6 wt.% Cu). After impregnation, the solids were dried overnight at 60 °C and calcined during 4 h at 400 °C. The catalysts were denoted 6CUMCE with M = Zr or Al according to the heteroatom added to the ceria. They were also denoted 6CUMCE-U (where -U = used) after catalytic activity.

2.2. Catalytic tests

Catalytic tests were carried out in a fixed bed reactor at atmospheric pressure. The catalysts (0.150 g), with a particle size (0.050–0.110 mm) were introduced into a tubular stainless steel reactor (5 mm i.d) controlled by interior place thermocouple in direct contact with the catalysts. The samples were pre-treated in-situ under flowing air for 30 min at 400 °C, followed by cooling to RT in He flow. The contact time W/F was 0.18 g s cm^{-3} (GHSV = 22,000 h^{-1}). The reaction mixture composition was 1.25% CO, 1.25% O_2, 50% H_2, balanced with He. The effect of CO_2 and H_2O was examined with the addition of 15% CO_2 and 12% H_2O. An ice-salt cooled cold finger was used to trap the water downstream from the reactor. A Shimadzu-GC-2014 gas chromatograph equipped with TCD, with a CP-Carboplot-P7 column, was used to analyze the outlet composition. The temperature was varied in the 65–190 °C range, and measurements were carried out till a steady state was achieved. Both methanation and reverse water–gas-shift reactions were found to be negligible in our experimental conditions. The carbon monoxide and oxygen conversions and the selectivity toward CO_2 were calculated as described elsewhere [8,9]. The excess of oxygen factor (λ) used was 2 because this value was previously found optimal for CO-PROX [8,9].

2.3. Characterization methods

X-ray diffraction (XRD) patterns were obtained with a Philips-X'Pert-PRO apparatus using $CuK_{\alpha 1}$ radiation ($\lambda = 0.1540$ nm). High resolution patterns were registered in order to apply the Rietveld method to estimate the average crystallite size.

Raman spectra were obtained using a BRUKER-RAM-II spectrometer with a Ge detector and the 1064 nm excitation line of Nd-YAG laser at N_2 liquid temperature. Powder samples were pressed into a small disc and mounted on the analysis chamber.

Hydrogen temperature-programmed reduction (H_2-TPR) experiments were carried out as described elsewhere [8,9] using 0.1 g of catalyst. Hydrogen consumption was calibrated with the reduction of a known amount of CuO.

X-ray photoelectron spectra (XPS) were collected using a Physical-Electronics PHI 5700 spectrometer with non monochromatic MgK_{α} radiation (300 W, 15 kV, 1253.6 eV). All spectra were referenced to the C 1s peak (284.8 eV) from the adventitious contamination layer. Short acquisition times of 10 min were used to examine Cu 2*p* and Ce 3*d* regions in order to avoid, as much as possible, photoreduction of Cu^{2+} species. Nevertheless, a Cu^{2+} reduction in high vacuum during the analysis cannot be excluded.

3. Results and discussion

3.1. Catalytic results

The catalytic activity of the 6CUMCE solids was evaluated in the CO-PROX reaction in H_2-rich feed, as relevant for the clean-up of reformate streams for PEMFC applications, in a temperature range of 65–190 °C (Fig. 1A).

The CO conversion of 6CUCE and 6CUALCE increases with the reaction temperature, reaching a conversion close to 100% at 140 °C for 6CUCE and 95% at 165 °C for 6CUALCE. 6CUZRCE exhibits its higher CO conversion value at 140 °C (87%), while at higher temperatures, the CO conversion diminishes dramatically. Considering the reaction stoichiometry, the oxygen excess factor used and the CO conversion values, the O_2 consumption is attributable to the oxidation of CO to CO_2. The selectivity to CO_2 is 100% until 90 °C, however the selectivity to CO_2 decreases at higher temperatures due to the competitive oxidation of H_2, which is in a much higher concentration [10].

The study of the catalytic stability was performed at 115 °C during 36 h under the usual operation temperatures of PEMFCs (Fig. 2). 6CUCE catalyst shows the highest conversion

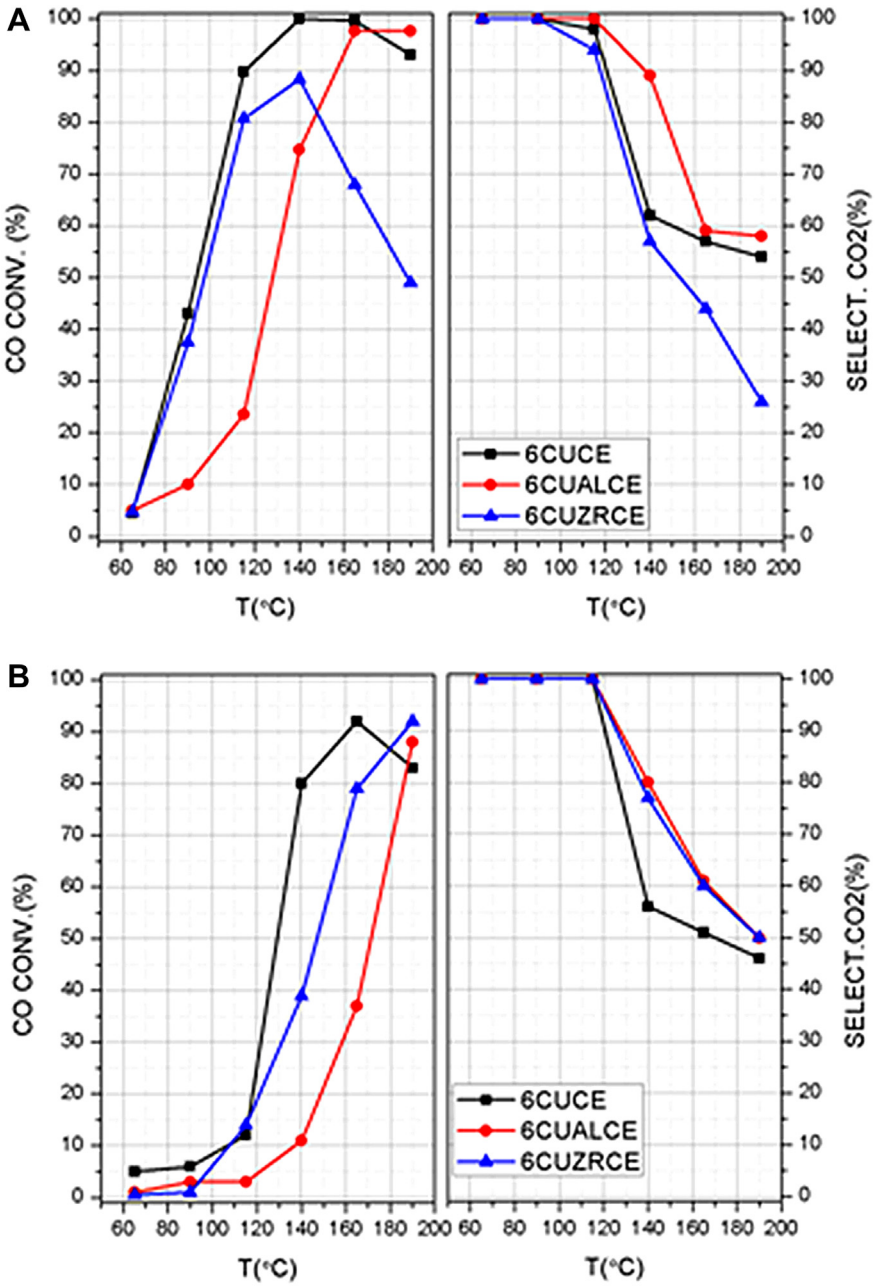

Fig. 1 – A: CO conversion and selectivity toward CO_2 as function of the temperature over the 6CUMCE. Operating conditions: GHSV = 22,000 h^{-1}, λ = 2, 1.25% CO, 1.25 %O_2, 50% H_2, He balance (%vol). B: CO conversion and selectivity toward CO_2 as function of the temperature over the 6CUMCE catalysts. Operating conditions: GHSV = 22000 h^{-1}, λ = 2, 1.25% CO, 1.25% O_2, 50% H_2, 15% CO_2, 12% H_2O, He balance (%vol).

maintaining a CO conversion close to 100% during 36 h on stream, while 6CUZRCE and 6CUALCE samples undergo a slightly progressive deactivation along the catalytic test. As regards to the CO_2 selectivity, all catalysts maintain their selectivity on the time on stream between 65 and 85%.

Finally, an additional catalytic test was carried out with the presence of both CO_2 and H_2O in the feed, simulating a PROX unit operation where the effluent coming from the water–gas shift still contains H_2O and CO_2 (Fig. 1B). As expected, the presence of CO_2 and H_2O in the gas stream affects the catalysts activity, leading to a decrease in CO conversion over the entire temperature range investigated. The trend of the catalytic activity is similar for all catalysts both in the absence and in the presence of CO_2 and H_2O, but shifted to a higher temperature [8,9]. The T50 value (temperature at which 50% CO conversion is observed) moves from 90 °C to 130 °C for 6CUCE, from 90 °C to 140 °C for 6CUZRCE and from 130 °C to 170 °C for 6CUALCE.

The presence of CO_2 reduces the CO conversion because adsorption of CO_2 on the active sites partially inhibits the CO adsorption. This inhibition is lower at higher temperatures and the CO conversion increases attaining conversion values

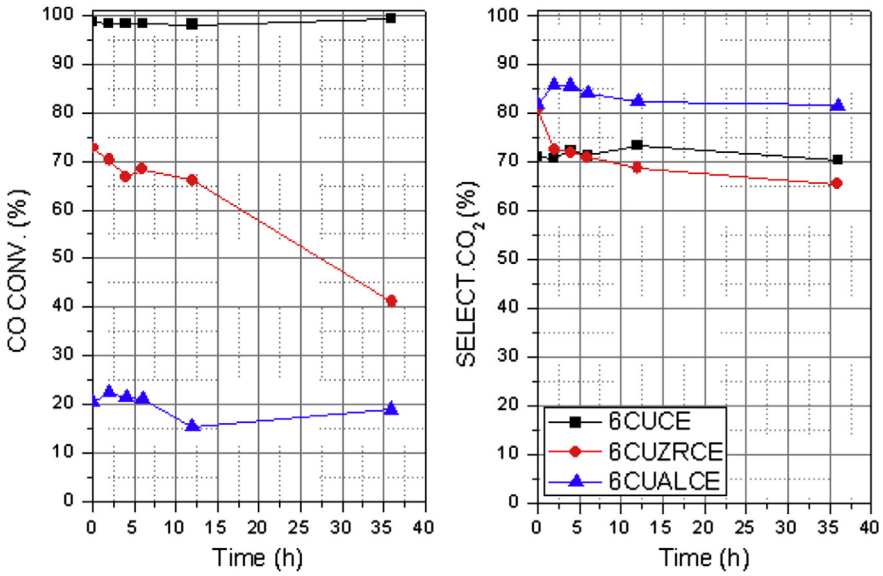

Fig. 2 – CO conversion of the 6CUMCE catalysts at 115 °C as a function of time on stream.

of about 90% due to CO_2 desorption at high temperatures, i.e., the equilibrium surface coverage is lower at higher temperatures [7]. The presence of water produces a blockage of the catalyst surface although from 140 °C all catalysts become more tolerant [7].

3.2. *Characterization and evolution of catalysts*

3.2.1. *XRD*

Fig. 3 compiles XRD patterns of the supports, fresh and spent catalysts. All samples show diffraction lines of CeO_2 ($2\theta = 28.5$, 33.4, 47.5 and 56.5°) assigned to cerianite (PDF 00-034-0394). $Ce_{0.8}Zr_{0.2}O_2$ and $Ce_{0.8}Al_{0.2}O_2$ diffractograms reveal the absence of ZrO_2 and Al_2O_3 phases, discarding the segregation of crystalline phases. $Ce_{0.8}Zr_{0.2}O_2$ exhibits a shift of the reflection lines of the cerianite phase to higher angles, revealing that zirconium species are into the ceria lattice forming a solid solution maintaining a cubic phase as was reported in the literature for low zirconium contains [11]. This shift is not noticeable for $Ce_{0.8}Al_{0.2}O_2$. Alumina is possibly in amorphous phase or in form of small crystallites undetectable by XRD.

Fresh catalysts diffractograms reveal the presence of diffraction lines corresponding to copper oxide (monoclinic tenorite) ($2\theta \approx 35.5$ and 39°) (PDF 00-048-1548) for 6CUALCE and 6CUZRCE, while for 6CUCE, the main diffraction lines of CuO are not detectable due to the small size and/or the very well-dispersed CuO particles. The incorporation of aluminum or zirconium to pure ceria generates a decrease of the dispersion of CuO in the surface of supports as indicates the increment of crystallite size of tenorite phase (24.4 nm for 6CUZRCE and 18.8 nm for 6CUALCE compared with the 15.7 nm of 6CUCE), estimated by Rietveld's method.

After CO-PROX tests, the used catalysts show the presence of new diffraction lines ($2\theta = 43.5$ and 50.4°) associated to Cu^0 (PDF 00-004-0836) with an average particle size of 155 nm for 6CUZRCE-U sample, suggesting that the deactivation of 6CUZRCE during CO-PROX reaction is caused by the reduction of copper oxide and its nucleation. Nevertheless for 6CUCE-U the particle size cannot be determined by Rietveld's method, meaning that a high dispersion is maintained ever after the catalytic test. 6CUALCE-U maintains similar crystallite size (about 18 nm) due to the strong interaction Al_2O_3–CuO that

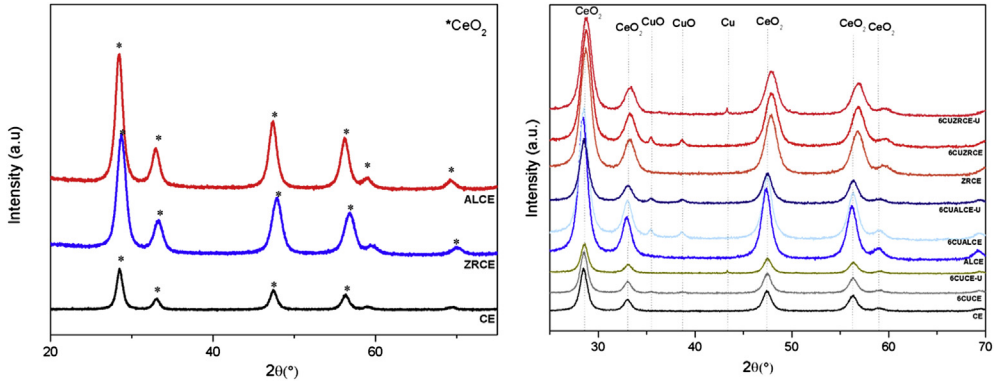

Fig. 3 – XRD patterns of supports (left) and catalysts (right) fresh and used synthesized.

leads to a lower reducibility of copper, corroborating the shift of the CO conversion at higher temperatures.

Lattice parameters were estimated by the Rietveld's method. CeO_2 and $Ce_{0.8}Al_{0.2}O_2$ show similar cell parameters ($a = 5.412$ Å) assigned to pure ceria, corroborating the absence of aluminum on the cerianite framework although alumina-ceria systems favors the stronger interaction between the support and the metal, high homogeneity and thermal stability [7]. Nevertheless, $Ce_{0.8}Zr_{0.2}O_2$ presents a lower cell parameter ($a = 5.365$ Å), typical of $Ce_{0.8}Zr_{0.2}O_2$ due to the lower atomic ratio of Zr^{4+} in comparison with Ce^{4+} which provokes a contraction of the lattice leading to a bigger strain enhancing the oxygen vacancies of the cerianite that improves the redox properties of ceria and provides a higher thermal stability [9–11]. For 6CUMCE, the strain and crystallite size of cerianite keeps almost unaltered, discarding the incorporation of copper to the ceria lattice, so CuO is present in the form of large segregated CuO particles (Fig. 3).

It is well known that in the ceria-based catalysts, the redox properties of the ceria support contribute to catalytic performance in CO-PROX in a very relevant way. In this particular case, the metal–support interaction can explain the differences among ceria, ceria–zirconia and ceria–alumina supports. The PROX-CO reaction takes place at the metal–support interface and the enhanced activity of the ceria-supported copper catalysts could arise from the very specific sites created at the copper nanoparticle perimeter [13]. Yet, the presence of larger copper particles diminishes the interface area, thus weakening the metal–support interaction. The XRD results show that the copper supported on ceria has smaller particles and greater dispersion than on the other two supports suggesting that the strong interaction between copper and ceria is responsible of the highest activity in the PROX-CO reaction of 6CUCE sample.

3.2.2. *Raman*

Raman spectrum of the CeO_2 support (not shown) reveals a main band around 470 cm^{-1} ascribed to the F_{2g} vibrational mode of the cubic fluorite structure of CeO_2 [14]. Similarly, $Ce_{0.8}Al_{0.2}O_2$ maintains the band at 470 cm^{-1} corroborating the absence of aluminum on the lattice ceria. The band is shifted toward higher wavenumber (476 cm^{-1}) for $Ce_{0.8}Zr_{0.2}O_2$ and becomes broader due to the Ce–Zr interaction by the modification of the strain by the incorporation of Zr^{4+} which exhibits lower atomic ratio than Ce^{4+} leads to an increasing of the vibration frequency of the metal-anion band.

Bands located at 295, 340 and 626 cm^{-1}, assigned to crystalline CuO bulk, is not noticeable which reveals a high dispersion of CuO over the support [15]. Finally, 6CUZRCE exhibits a very weak band 600 cm^{-1} assigned to the oxygen vacancies in the structure [9], indicating the existence of Ce^{3+} ions due to the contraction of the lattice by the incorporation of Zr^{4+} that favors the oxygen mobility improving the redox properties.

3.2.3. *Redox properties*

Redox properties were analyzed by H_2-TPR (Fig. 4). The reduction of CeO_2 occurs in two regions. The first region (285–675 °C) assigned to coordinately unsaturated surface capping oxygen ions is favored for lower particle size obtained by freezing-dry method and the second region (675–950 °C) is attributed to bulk oxygen that requires to be transported to the surface before their reduction. $Ce_{0.8}Zr_{0.2}O_2$ undergoes reduction in one step (400–800 °C) suggesting that the entire ceria is present in the solid solution improving the oxygen-storage capacity [11]. A $Ce_{0.8}Al_{0.2}O_2$ shows two regions but shifted to higher temperatures than CeO_2 due to the strong interaction CeO_2–Al_2O_3, the first (400–900 °C) is attributed to the reduction process of the surface ceria and the second at 940 °C to the conversion of a partially reduced $CeAlO_3$ [16].

The reduction of bulk CuO occurs at about 380 °C (not shown). For 6CUMCE reduction peaks are shifted to lower temperatures (150–250 °C) due to spillover process promoted by CuO–CeO_2 interfacial sites (Fig. 3B) [17]. H_2-TPR profiles have been decomposed in α peak, assigned to the reduction of CuO dispersed in close contact with CeO_2 surface typical for low copper content (<3%wt. Cu), β peak, assigned to CuO species highly dispersed and strongly interacting with CeO_2 is typical of higher copper content and γ peak that has been assigned to bulk copper oxide species which are associated with ceria [6,14]. 6CUCE and 6CUZRCE exhibit a small α peak at ~150 °C and the β peak more intense about 197 °C become larger. CuO species reduced in both cases being more intense for 6CUZRCE by the presence of more oxygen vacancies that increases the redox properties of the catalytic system. For 6CUCE, it also detected a small shoulder assigned γ peak due to the reduction of bulk CuO [8,10]. 6CUALCE catalyst exhibits

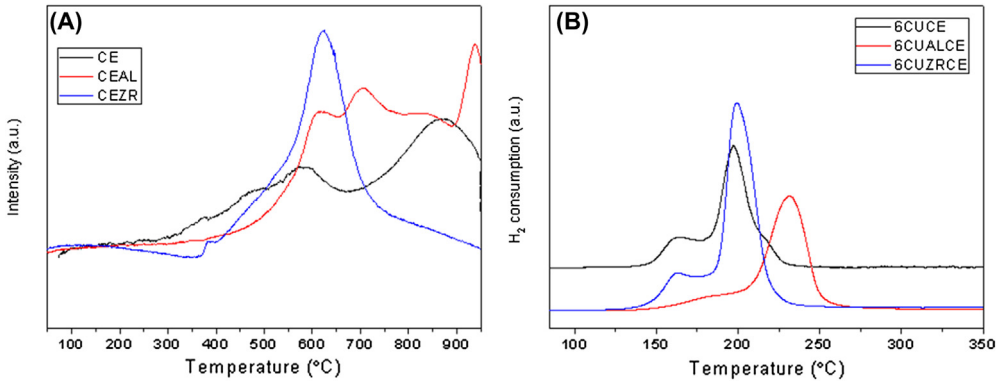

Fig. 4 – H_2-TPR of supports (A) and fresh catalysts (B).

Table 1 – Reducibility degree for 6CUMCE catalysts obtained by H_2-TPR.

Sample	Peak α (%)	Peak β (%)	Peak γ (%)	$\beta+\gamma$	$\alpha/\beta+\gamma$	H_2 uptake (μmol g^{-1})	H_2/Cu (mol mol^{-1})
6CUCE	24.6	59.3	16	75.3	0.33	907	1.20
6CUALCE	18.8	81.2	–	81.2	0.23	1074	1.42
6CUZRCE	27.2	72.8	–	72.8	0.37	1660	2.19

a shift of both α peak and β peak at higher temperatures by the hard interaction CuO–Al_2O_3 that diminishes the reducibility of the copper (Table 1).

In summary, the reduction temperature of copper species is lower for 6CUCE and 6CUZRCE than for 6CUALCE due to CuO particles supported on CeO_2–Al_2O_3 are less reducible by a stronger interaction CuO–Al_2O_3, corroborating XRD analyzes, where 6CUALCE and 6CUALCE-U showed the absence of reduced copper in the used sample, despite the operating conditions in a reducing atmosphere (50% H_2). TPR results also corroborate the lower conversion in CO-PROX reaction shown by the CeO_2–Al_2O_3 based system.

Quantitative analysis of H_2 consumption for 6CUMCE is shown in Table 1. Theoretical consumption of H_2 to the reduction of CuO bulk is 755 μmol g^{-1} H_2. The molar ratio H_2/Cu underlines that the H_2 consumption is higher than the necessary for the theoretical complete reduction of copper in all samples, assuming all copper in the catalysts is reduced in H_2-TPR, a significant amount of the oxygen ions of the ceria is also reduced, this fact is enhanced for 6CUZRCE by an increasing the surface oxygen vacancies [10].

3.2.4. XPS

The surface composition and the oxidation state of the catalysts were studied by XPS (see Table 2). The surface atomic ratios Cu/Ce of fresh samples ranged from 0.47 for 6CUZRCE to 0.70 for 6CUALCE, being 0.57 for 6CUCE, revealing a lower dispersion for 6CUZRCE. For spent catalysts, these surface atomic ratios Cu/Ce ranged from 0.66 for 6CUALCE to 2.28 for 6CUZRCE, being 1.02 for 6CUCE. The redox parameters indicates a partial reduction of Ce^{4+} for 6CUCE, however this catalyst presents the highest catalytic results due to this catalyst maintain the dispersion of the copper sites.

Table 2 – Binding energies and redox parameters of fresh and spent catalysts.

Sample	Cu $2p_{3/2}$ (eV)	Cu_{red}/Cu	I_{sat}/I_{pp}	Ce^{3+}/Ce^{4+}
6CUCE	932.8 (81.2%)	0.82	0.36	0.32
	934.8 (18.1%)			
6CUCE-U	933.1 (86.7%)	0.87	0.31	0.40
	935.4 (13.3%)			
6CUALCE	932.9 (72.9%)	0.73	0.36	0.24
	934.9 (27.1%)			
6ALCUCE-U	932.7 (59.5%)	0.75	0.54	0.25
	934.8 (40.5%)			
6CUZRCE	932.8 (63.2%)	0.68	0.45	0.17
	934.7 (36.8%)			
6CUZRCE-U	932.9 (59.6%)	0.68	0.49	0.17
	934.8 (40,4%)			

The Ce 3*d* spectra can be decomposed in ten contributions: *v*, *u* (Ce $3d^9$ $4f^2$ O $2p^4$) and *v″*, *u″* (Ce $3d^9$ $4f^1$ O $2p^5$); *v‴*, *u‴* (final state of Ce $3d^9$ $4f^0$ O $2p^6$) assigned to Ce(IV); v_0,u_0 (Ce $3d^9$ $4f^2$ O $2p^5$) and *v′*, *u′* (Ce $3d^9$ $4f^1$ O $2p^6$) assigned to Ce(III) as a consequence of the hybridization between the Ce 4*f* levels and the O 2*p* states [18]. For 6CUMCE, Cu 2*p* region shows two contributions located at 934.8 eV assigned to Cu^{2+} species and 934.8 eV attributed to Cu reduced species, along with the shake-up peak above Cu^{2+} species at 942.1 eV, so it must suppose that copper is present as CuO and/or Cu_2O [19]. Spent catalysts show a decrease in the Cu^{2+} signal due to H_2-rich feed, being possible the superficial re-oxidation after the CO-PROX reaction, corroborating XRD and H_2-TPR data. The redox parameters indicates a partial reduction of Ce^{4+} for 6CUCE, despite this catalyst presents the highest catalytic results due to the high dispersion of the copper sites. However 6CUALCE and 6CUZRCE exhibit lower degree of Ce^{4+}, suggesting that the incorporation of aluminum or zirconium provides stability to ceria although both catalysts show lower catalytic results due to the lower dispersion in 6CUZRCE and the hard interaction CuO–Al_2O_3 in 6CUALCE as was reported in H_2-TPR. Finally, the C 1s region of 6CUMCE-U show a peak at 288.6 eV assigned to the presence of carbonates due to the CO_2 adsorption on the active phase [6], being more appreciable for 6CUZRCE according to the catalytic results.

4. Conclusions

6CUMCE catalysts were synthesized by freeze-drying method, characterized and tested for CO-PROX reaction. This synthetic method generates ceria with a low particle size, a strong interaction support-CuO and a high dispersion. The incorporation of metal doping in the lattice of CeO_2 produces modifications in the redox properties that affect the behavior in the CO-PROX reaction.

6CUALCE exhibits the lowest conversion due to needs to operate at higher temperatures to obtain high conversion values by a strong interaction CuO–Al_2O_3, as revealed H_2-TPR measurements, where α and β peaks is shifted at higher temperatures, compared with the other samples, diminishing the reducibility of the copper species responsible for catalytic activity.

Acknowledgments

This work was supported by the project CTQ2012-37925-C03-03, MAT2007-60127 and MAT2010-16007 (Ministerio de Ciencia e Innovación, Spain and FEDER Funds) and by the project FQM01661 (Junta de Andalucía, Spain).

REFERENCES

[1] Minh NQ, Takahashi T. Electrolyte science and technology of ceramic fuel cells. Amsterdam: Elsevier; 1995.

[2] Stark JV, Klabunde KJ. Nanoscale metal oxide particles/clusters as chemical reagents. Adsorption of hydrogen halides, nitric oxide, and sulfur trioxide on magnesium oxide nanocrystals and compared with microcrystals. Chem Mater 1996;8:1913–8.

[3] Lindström B, Pettersson LJ. Hydrogen generation by steam reforming of methanol over copper-based catalysts for fuel cell applications. Int J Hydrogen Energy 2001;26:923–33.

[4] Morse JD. Micro-fuel cell power sources. Int J Energy Res 2007;31:576–602.

[5] Avgouropoulos G, Ioannides T. Effect of synthesis parameters on catalytic properties of CuO CeO_2. Appl Catal B Environ 2006;67:1–11.

[6] Ayastui JL, Gurbani A, González-Marcos MP, Gutíerrez-Ortiz MA. Effect of copper loading on copper-ceria catalysts performance in CO selective oxidation for fuel cell applications. Int J Hydrogen Energy 2010;35:1232–44.

[7] Gamarra D, Martínez-Arias A. Preferential oxidation of CO in rich H_2 over CuO/CeO_2: operando-DRIFTS analysis of deactivating effect of CO_2 and H_2O. J Catal 2009;263:189–95.

[8] Moretti E, Lenarda M, Storaro L, Talon A, Montanari T, Busca G, et al. One-step synthesis of a structurally organized mesoporous $CuO\text{-}CeO_2\text{-}Al_2O_3$ system for the preferential CO oxidation. Appl Catal A Gen 2008;335:46–55.

[9] Moretti E, Storaro L, Talon A, Lenarda M, Riello P, Frattini, et al. Effect of thermal treatments on the catalytic behaviour in the CO preferential oxidation of a $CuO–CeO_2–ZrO_2$ catalyst with a flower-like morphology. Appl Catal B Environ 2011;112:627–37.

[10] DiMonte R, Kaspar J. Nanostructured $CeO_2\text{-}ZrO_2$ mixed oxides. J Mater Chem 2005;15:633–48.

[11] Ayastui JL, Gurbani A, González-Marcos MP, Gutíerrez-Ortiz MA. Selective CO oxidation in H_2 streams on $CuO/Ce_xZr_{1-x}O_2$ catalysts: correlation between activity and low temperature reducibility. Int J Hydrogen Energy 2012;37:1993–2006.

[12] Perez-Coll D, Nunez P, Frade JR, Abrantes JCC. Conductivity of CGO and CSO ceramics obtained from freeze-dried precursors. Electrochim Acta 2003;48:1551–7.

[13] Mariño F, Descorme C, Duprez D. Supported base metal catalysis for the preferential oxidation of carbon monoxide in the presence of excess hydrogen (PROX). Appl Catal B Environ 2005;58:175–83.

[14] Marbán G, Fuentes AB. Highly active and selective CuO_x/CeO_2 catalyst prepared by a single-step citrate method for preferential oxidation of carbon monoxide. Appl Catal B Environ 2005;57:43–53.

[15] Yu JF, Ji W, Shen ZX, Li WS, Tang SH, Ye XR, et al. Raman spectra of CuO nanocrystal. J Raman Spectrosc 1999;30:413–5.

[16] Shyu JZ, Weber WH, Gandhi HS. Surface characterization of alumina-supported ceria. J Phys Chem 1988;92:4964–70.

[17] Bera P, Priolkar KR, Sarode PR, Hedge MS, Emura S, Kumashiro R. Structural investigation of combustion synthesized Cu/CeO_2 catalysts by EXAFS and other physical techniques: formation of a $Ce_{1-x}Cu_xO_{2-\delta}$ solid solution. Chem Mater 2002;14:3591–601.

[18] Zhang F, Wang P, Koberstein J, Khalid S, Chan SW. Cerium oxide state in ceria nanoparticles studied with X-ray photoelectron spectroscopy and adsorption near edge spectroscopy. Surf Sci 2004;563:74–82.

[19] Tang X, Zhang B, Li Y, Xu Y, Xin Q, Shen W. CuO/CeO_2 catalysts: redox features and catalytic behaviors. Appl Catal A Gen 2005;288:116–25.